AIP Journal of Applied Physics

Characterization of the insulator barrier and the superconducting transition temperature in GdBa2Cu3O7−δ/BaTiO3 bilayers for application in tunnel junctions

H. Navarro, Ilkyu Yang, M. Sirena, Jeehoon Kim, and N. Haberkorn

Citation: Journal of Applied Physics **118**, 045308 (2015); doi: 10.1063/1.4927751
View online: http://dx.doi.org/10.1063/1.4927751
View Table of Contents: http://scitation.aip.org/content/aip/journal/jap/118/4?ver=pdfcov
Published by the AIP Publishing

Characterization of the insulator barrier and the superconducting transition temperature in $GdBa_2Cu_3O_{7-\delta}/BaTiO_3$ bilayers for application in tunnel junctions

H. Navarro,[1,2,a)] Ilkyu Yang,[3] M. Sirena,[1,2] Jeehoon Kim,[3,4] and N. Haberkorn[1,2]
[1]*Instituto Balseiro, Universidad Nacional de Cuyo and CNEA, 8400 Bariloche, Argentina*
[2]*Centro Atómico Bariloche, Comisión Nacional de Energía Atómica. Av. Bustillo 9500, 8400 San Carlos de Bariloche, Argentina*
[3]*Department of Physics, Pohang University of Science and Technology, Pohang, South Korea*
[4]*CALDES, Institute for Basic Science, Pohang, South Korea*

(Received 26 February 2015; accepted 21 July 2015; published online 30 July 2015)

The optimization of the superconducting properties in a bottom electrode and the quality of an insulator barrier are the first steps in the development of superconductor/insulator/superconductor tunnel junctions. Here, we study the quality of a $BaTiO_3$ tunnel barrier deposited on a 16 nm thick $GdBa_2Cu_3O_{7-\delta}$ thin film by using conductive atomic force microscopy. We find that the tunnel current is systematically reduced (for equal applied voltage) by increasing the $BaTiO_3$ barrier thickness between 1.6 and 4 nm. The $BaTiO_3$ layers present an energy barrier of ≈1.2 eV and an attenuation length of 0.35–0.5 nm (depending on the applied voltage). The $GdBa_2Cu_3O_{7-\delta}$ electrode is totally covered by a $BaTiO_3$ thickness above 3 nm. The presence of ferroelectricity was verified by piezoresponse force microscopy for a 4 nm thick $BaTiO_3$ top layer. The superconducting transition temperature of the bilayers is systematically suppressed by increasing the $BaTiO_3$ thickness. This fact can be associated with stress at the interface and a reduction of the orthorhombicity of the $GdBa_2Cu_3O_{7-\delta}$. The reduction in the orthorhombicity is expected by considering the interface mismatch and it can also be affected by reduced oxygen stoichiometry (poor oxygen diffusion across the $BaTiO_3$ barrier). © *2015 AIP Publishing LLC*.
[http://dx.doi.org/10.1063/1.4927751]

I. INTRODUCTION

Superconductor–Insulator–Superconductor (SIS) tunnel junctions based on high temperature superconductors (HTS) have potential applications such as magnetometers,[1] voltage standards,[2] logic,[3] and qubits.[4] High superconducting transition temperature (T_s) and large band gap, in comparison with conventional low temperature superconductors (LTS), offer advantages over, for example, niobium.[5] The design of such tunnel junctions using thin films based on copper oxides requires a particular attention in the quality of the materials. This attention must be focused on the topology and the effect of the disorder on the intrinsic properties of the materials. The control of the topology in the bottom superconducting layer (flat surfaces) is necessary to avoid pinholes in the thin dielectric layer. The tunnel barrier should be an insulator and should also ensure a small mismatch with the superconducting material (top electrode). For SIS, the conductance of the barrier is determined by the barrier thickness (d), its energy barrier height (ϕ), and the attenuation length (λ).[6] Furthermore, the performance of the SIS tunnel junction is limited by the coupling between the superconducting electrodes, which makes it necessary to understand how the disorder mechanisms modify the intrinsic electronic and magnetic properties of the materials at the interfaces.[7,8]

Among the different materials suited for tunnel barriers, $Ba_{1-x}Sr_xTiO_3$ (BSTO) is a candidate due to its chemical compatibility and the small lattice mismatch with a variety of structures such as $RBa_2Cu_3O_{7-\delta}$ (RBCO; R: Y, Gd, and Eu). New functionalities of the tunnel junction can be also expected by using ferroelectric (FE) and ferromagnetic (FM) materials for the barrier.[9,10] For example, the interaction between superconductivity and FE reduces T_s and affects the superconducting gap,[11] which makes the design of SIS tunnel junctions with tunable properties possible.[12] The dielectric properties of $Ba_{1-x}Sr_xTiO_3$ (BSTO) have been extensively studied.[13–15] Pure $SrTiO_3$ (STO) and $BaTiO_3$ (BTO) are insulators with a wide band gap of 3.2 eV and ≅3 eV, respectively.[16,17] STO is an incipient FE (quantum paraelectric material) with a soft polar mode characterized by the suppression of the FE phase transition at low temperatures.[18] BTO presents three consecutive phase transitions: first, from cubic $m3m$ to the tetragonal 4 mm phase at 403 K; then, to the orthorhombic mm^2 phase at 278 K; and finally, to the rhombohedral 3 m phase at 183 K.[13] The lattice parameter in BSTO is given by the doping x, and it changes from 0.3905 (STO) to 0.399 nm (BTO). The change in the lattice parameter is approximately equal to $0.399–1 \times 10^{-3}\ x$ (nm). The FE properties depend on the doping and are affected by stress. For instance, FE is induced by strain in STO,[19] whereas the Curie temperature (T_c) is increased by strain in BTO.[20] On the other hand, the FE properties of very thin BSTO films are also affected by the dimensionality. The

a)Author to whom correspondence should be addressed. Electronic mail: henrynavarro@cab.cnea.gov.ar. Tel.: +54 0294 444 5171. FAX: +54 0294 444 5299.

theoretical critical thickness calculated for FE in BTO is around 2 nm.[21,22]

Here, we report the resulting structural and electrical properties of very-thin BTO insulator layers in $GdBa_2Cu_3O_{7-\delta}$ (GBCO)/BTO bilayers. BTO top layers with thicknesses of 1.6 nm, 2 nm, 3 nm, and 4 nm were grown on 16 nm thick GBCO thin films. The BTO tunnel-barrier was characterized by using a conductive atomic force microscope (CAFM). It was noticed that the tunnel current is systematically reduced (for the same applied voltage) by increasing the BTO barrier. The BTO layers present values of $\phi \approx 1.2$ eV and $\lambda \approx 0.35$–0.5 nm (depending on voltage). The presence of FE was verified by piezoresponse force microscopy (PFM) for a BTO thickness of 4 nm. The T_s of the bilayers is systematically suppressed by increasing the BTO thickness, which can be associated with reduced orthorhombicity in the GBCO electrode by changes in the oxygen stoichiometry.[23–25]

II. EXPERIMENTAL METHODS

The GBCO/BTO bilayers were grown on (100) STO substrates by DC magnetron and RF sputtering, respectively. The deposition temperature was 710 °C (T_D). The target power was 25 W and the total pressure at the chamber was 400 mTorr (90:10, argon:oxygen). A 2 nm thick STO buffer layer was previously placed on the substrate in order to reduce the 3D growth of the GBCO films.[26] Prior to the deposition, the STO substrate was heated in air at 900 °C for 20 min to reduce its organic contamination and to clean its surfaces. During the growth, the not aligned chopped power oscillatory (NACHOS) configurations were used.[27] The GBCO growth rate was 1.6 nm/min. The STO and BTO growth rate were 1 nm/min. The GBCO thickness was fixed at 16 nm. Bilayers with BTO final thicknesses (d_{BTO}) of 1.6 nm, 2 nm, 3 nm, and 4 nm were grown by using identical deposition conditions. At the end of the sputtering process, the substrate was cooled down to 500 °C, and the chamber was flooded with pure oxygen at a pressure of 100 Torr. Then, the films were cooled down to room temperature at a rate of 1 °C/min. Wherever used, the notation [G-B-d_{BTO}] indicates a GBCO layer with a thickness of 16 nm and BTO layer with thickness d (nm).

The structure of the films was analyzed by X-ray diffractometry (XRD) using a Panalytical Empyrean equipment. CAFM measurements were performed in a Dimension 3100 Brucker microscope, using diamond doped conductive tips. The samples were imaged in air at room temperature within the following 24 h after the sample growth. The topographical and electronic properties of the BTO layer were performed by analyzing the topographic and CAFM information at different scales (1 μm and 10 μm). Measurements were made in contact mode at constant force.[28] The minimum detectable current in the CAFM used was 50 pA, and the maximum current was 480 nA, under a bias voltage ranging from 0.01 to 12 V. The CAFM was operated with a constant force (0.5 V of deflection set point), the laser always reflecting the same position of the cantilever, and with a constant bias voltage to reduce fluctuations in the mapping of the tunnel currents as a consequence of external parameters.[6] PFM measurement in the [G-B-4] bilayer was carried out in UHV-SPM system (Omicron) with NSC35B:HQ tip (Mikromasch).

The superconducting transition temperature was obtained by performing magnetization versus temperature measurements in a commercial superconducting quantum interference device (SQUID). A magnetic field (H) of 1.5 Oe was perpendicularly applied to the surface of the films after cooling the sample down in zero field (ZFC). T_s was defined as the end of the diamagnetic transition (zero magnetization).

III. RESULTS AND DISCUSSION

The crystalline structure of the [G-B-d_{BTO}] bilayers was examined by XRD and was found to be single phase with a (00l) orientation (not shown).[26] No additional peaks due to secondary phases or different crystalline orientations were observed. The rocking curve for [G-B-4] along the (005) GBCO and (001) BTO reflections were 0.42° and 0.46°, respectively. The calculated BTO out-plane lattice parameter, obtained from the (001) reflection, was 0.420 (2) nm. The matching of the lattice parameters at the interfaces without the presence of dislocations implies that optimal oxygen doping in the GBCO layer (lattice parameters $a_{GBCO} = 0.383$ nm and $b_{GBCO} = 0.389$ nm) can only be achieved by in-plane constrained BTO. As expected, the estimated in-plane lattice parameter for BTO, considering unit-cell volume–conservation, was around 0.388 (2) nm.

Figure 1 shows topography images and current maps for [G-B-1.6], [G-B-2], [G-B-3], and [G-B-4] in areas of 10×10 μm^2. Pure GBCO thin films were previously analyzed in Ref. 29. The three dimensional (3D) nucleation in the 16 nm thick GBCO film was strongly reduced by including a STO buffer layer. The bilayers display a surface topology with uniform terraces and a roughness average (Ra) (expressed as root mean square (RMS)) between 1 and 2 nm, except for [G-B-3] where the RMS is close to 3 nm (see Table I). The heights of the steps at the border of the terraces range from 1 to 7 nm. The CAFM image of the pure electrode has been previously discussed.[26] CAFM images obtained by applying 4.4 V show that as the thickness of the BTO increases, the tunneling current decreases. We will define pinholes as the regions with current I > 440 nA. It is important to mention that current saturation occurs in both holes in the barrier and hot spots (very thin barrier). The density of surface defects (P_d defined as the percent fraction of points with saturation current I > 440 nA) from CAFM images is systematically reduced: 7.5% ([G-B-1.6]), 0.3% [G-B-2], 0.05% ([G-B-3]), and no pinholes (current saturation) were observed in [G-B-4] (see Table I). Figure 2 shows a correlation between the topography and CAFM in areas with and without 3D surface defects in [G-B-1.6], [G-B-2], and [G-B-3] (samples with pinholes). As observed in Fig. 2(a), [G-B-1.6] shows high conductivity in the entire surface. On the other hand, signatures of pinholes with saturation of the current ($I = 480$ nA) are observed at the borders of the terraces (steps of 3 nm) and on 3D surface defects. The increment of the BTO thickness ([G-B-2]) reduces the conductivity on smooth surfaces. However, the pinholes at the borders of the terraces are not covered. Finally, in

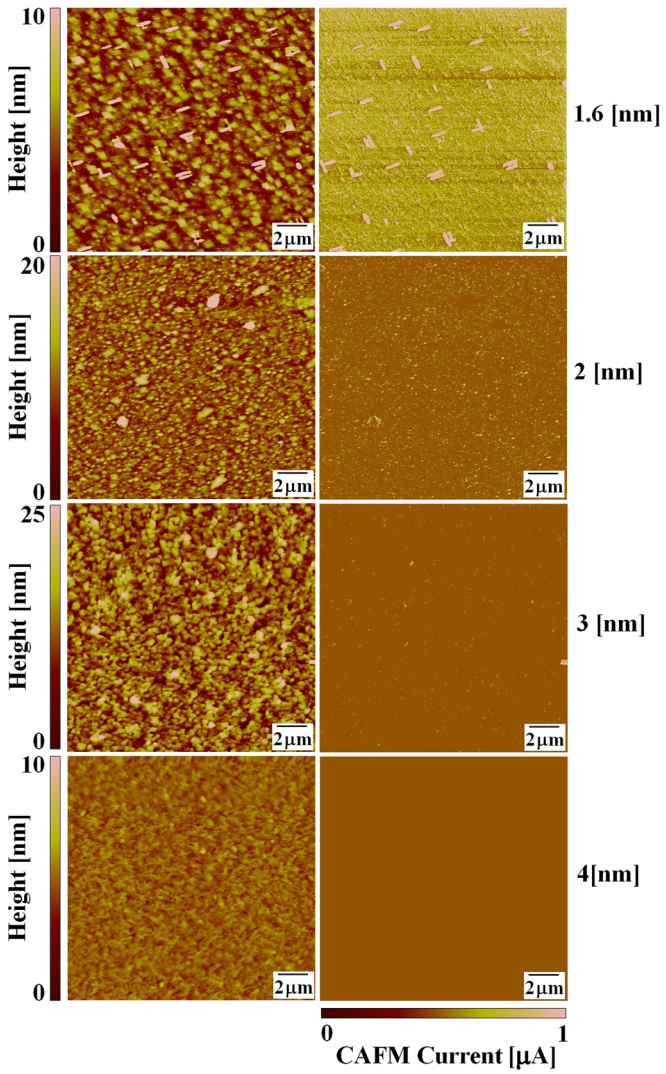

FIG. 1. Topology (left) and CAFM (right) $10 \times 10\,\mu m^2$ images of the [G-B-1.6], [G-B-2], [G-B-3], and [G-B-4] bilayers (from the top to the bottom, respectively).

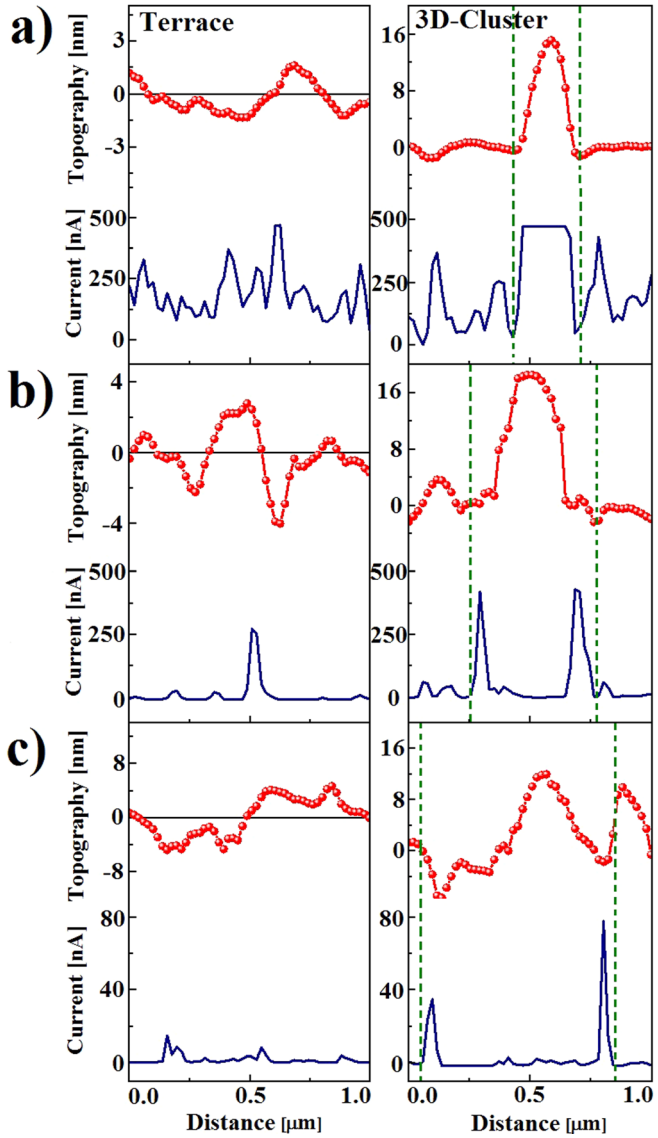

FIG. 2. AFM and CAFM profiles of regions with (left) and without (right) surface 3D defects. (a) [G-B-1.6], (b) [G-B-2], and (c) [G-B-3].

[G-B-3], the current around borders of the terraces and 3D defects is systematically reduced (in comparison with Figs. 2(a) and 2(b). Mainly, Fig. 2 indicates that although the tunneling current is reduced by increasing the BTO thickness, the quality of the barrier in areas of $10 \times 10\,\mu m$ (typical for real tunnel junctions) is limited by the imperfections generated by the roughness of the bottom electrode (pinholes or region with high conductivity).[29]

Figure 3 shows the CAFM current distributions for the [G-B-d_{BTO}] bilayers obtained from Fig. 1. The log-normal

TABLE I. Summary of the topographic and electronic properties in the studied bilayers (RMS: root mean square; T_s: superconducting critical transition; ad P_d (%): density of pinholes defined as the percent fraction of points with saturation current I > 440 nA).

Sample	RMS	T_s (K)	P_d (%)
[G-B-1.6]	1.2 nm	75 (1)	7.5
[G-B-2]	1.7 nm	74 (1)	0.3
[G-B-3]	2.9 nm	60 (2)	0.05
[G-B-4]	1.6 nm	48 (2)	0

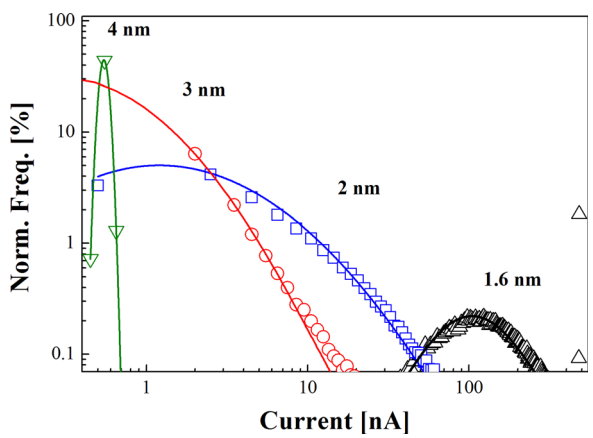

FIG. 3. Current distributions for GBCO/BTO bilayers for different BTO thicknesses with Voltage = 4.4 V. The lines correspond to the fittings using a log-normal distribution.

distribution was applied to fit the distribution of data.[30] The current distribution shifts to lower values when the BTO thickness is increased. The high density of points at the saturation region in [G-B-1.6] corresponds to pinholes produced by the terrace borders and the 3D surface defects. The mean current decays exponentially as the insulator layer thickness increases (see inset Fig. 4). This effect could be related to the presence of pinholes in the barrier[31] and/or tunneling transport of the electrons.[32] However, it be should noted that I-V curves taken over the insulator barrier (see Fig. 4) also give an exponential decay of the current with thickness of barrier. This suggests that tunneling could be the main mechanism for electronic transport thought the insulator barrier. The wide distribution of currents with a log-normal distribution can be attributed to thickness fluctuations of the barrier. The distribution of currents in the bilayers with thin BTO insulating barriers can be also strongly affected by small fluctuations in the BTO thickness (± 1 u. c.) and by the presence of different stacking sequences at the interface.[33] Different barrier properties can be expected by considering different stacking sequences of planes between GBCO ($CuO\text{-}BaO\text{-}CuO_2\text{-}Gd$) and BTO ($BaO\text{-}TiO_2$).

Figure 4 shows current (I) vs. voltage (V) in the different [G-B-d_{BTO}] bilayers. The curves correspond to the average of 20–30 measurements in different places of the samples. The I-V curve of a GBCO electrode was discussed in Ref. 29 and provides information about the conductance associated to pinholes in the bilayers. The GBCO electrode presents a non-linear behavior of the current voltage characteristics, which is usually observed in oxide electrodes due to the passivation of the surface. The current saturates ($I = 480$ nA) at $V < 0.5$ V. The curves for the bilayers present power-law dependences. This is in agreement with tunneling across an insulator barrier and is well described by the model of Simmons,[34] where $I\ (V,\ d) = I_0 V^{\alpha} e^{-d/\lambda}$ (λ is the attenuation length of the charge carriers in the barrier).[6] Short attenuation lengths correspond to high insulating barriers (fast decay of the tunneling current). The theoretical model considers $\alpha_0 = 2$ for tunneling at the high voltage regime ($V > \phi$, where

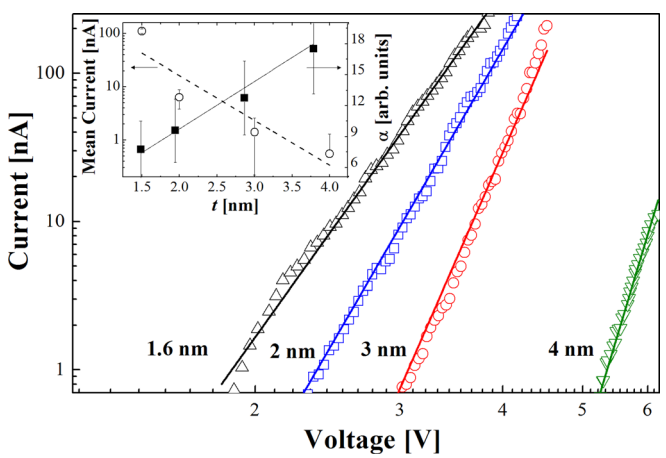

FIG. 4. Current (I) vs voltage (V) curves for the [G-B-1.6], [G-B-2], [G-B-3], and [G-B-4] bilayers. The solid lines correspond to linear fits by using: $I\ (V,\ d) = I_0 V^{\alpha} e^{-d/\lambda}$. The inset displays the thickness dependence of α (fit) and the mean current obtained from CAFM images by applying 4.4 V.

ϕ is the energy barrier). In our case, $\alpha_0 = 1.5$ (0.5) has been estimated (see inset Fig. 2). On the other hand, to obtain λ, $\mathrm{Ln}(I/V^{\alpha 0}) = a_0 - d/\lambda$ was plotted as a function of d for different polarization voltages V, and being λ between 0.35 nm (3 V) and 0.5 nm (3.9 V) ($\approx$1 BTO u. c.). Considering the λ values, the energy barrier can by estimated for different voltages. Considering a rectangular shape, the energy barrier is given by $\phi = \left(\frac{3he}{8\pi\sqrt{2m^*}}\frac{V}{\lambda}\right)^{2/3}$, where h is the Planck constant, m^* is the effective mass of the charge carriers, e is the electron charge, and V is the applied voltage. For the present estimation, $m^* = 6.5\, m_e$,[35] could be considered, giving an estimated energy barrier of 0.6 eV, for an applied voltage between 3 and 3.8 V. This value is slightly higher to those reported in $La_{0.67}Ca_{0.33}MnO_3$/STO ($\approx$0.23 eV) and GBCO/STO ($\approx$0.5 eV, for $m^* = 6\, m_e$) bilayers obtained by pulsed laser deposition and DC sputtering.[29,32] It is important to mention that, in comparison with bulk samples, the value m^* in a thin layer can be reduced by disorder. For the limit of $m^* \rightarrow m_e$, we obtain $\phi \approx 1.2$ eV. The expected barrier height can be estimated by considering the CAFM tip/BTO/GBCO barrier.[32] For an insulator without defects, in the absence of trapped charge (Schottky limit) and with a GBCO positively biased ($V > \phi/e$), the barrier between the BTO and the GBCO can be estimated as the difference between the work function of the GBCO (w_{GBCO}) and the electron affinity of the BTO (χ_{BTO}). By considering $w_{GBCO} = 6.1$ eV and $\chi_{BTO} = 3.9$ eV,[36,37] ϕ is expected to be no larger than 2.2 eV. This value is higher than the data estimated from the experimental I-V curves. Disorder mechanisms, such as nonstoichiometric Ba/Ti ratio and oxygen vacancies, usually increase the conductivity in BTO.[38,39] Furthermore, disorder at the interfaces can modify the properties in comparison to bulk materials. In order to verify the increment of the metallicity by changes in the oxygen vacancies, CAFM measurements were performed in a [G-B-d_{BTO}] bilayer growth in similar conditions, but the samples were cooled down from 500 °C in oxygen pressure of 1 Torr instead of 100 Torr. It is known that oxygen pressure also modifies the properties of the GBCO electrodes.[24] The obtained results show a higher conductivity across the BTO. For example, the mean currents (from the I-V curves) at 4 V in samples with 4 nm thick BTO are $\approx$30 nA (not shown) and below 1 nA for the samples cooled down in oxygen pressures of 1 and 100 Torr, respectively. On the other hand, ϕ decreases around 20% in the desoxygenated samples. In this context, the electronic properties of the barrier are extremely sensitive to the experimental conditions. The effect can be more relevant in GBCO/BTO/GBCO trilayers, where the oxygenation of the barrier and the bottom GBCO electrode imply oxygen diffusion across the top superconducting electrode. It is important to mention that full oxygenation without suppression of the superconducting properties at the GBCO/BTO interface is necessary for an effective superconducting coupling in tunnel junctions.

The absence of pinholes in [G-B-4] suggests that under the growth conditions here presented, 4 nm thick BTO have potential applications for the design of GBCO/BTO/GBCO tunnel junctions. As described in the introduction, the

presence of FE in BTO is affected by the dimensionality of the samples. In order to verify the presence of FE in the [G-B-4] bilayer, a bi-domain polarization image was obtained at room temperature (see Fig. 5). The scan area corresponds to $3.5 \times 3.5\ \mu m^2$. Domains with polarization down ($2 \times 2\ \mu m^2$) and up ($1 \times 1\ \mu m^2$) were written by applying −4 V and 4 V, respectively. For the PFM measurement, the AC probing voltage at 13 kHz was 1.5 V. The presence of FE for 4 nm thick BTO was confirmed switching the polarization states (up and down) by external bias at the different domains (see dotted lines squares in Fig. 5(b)). No correlation between the topology and the polarization states was observed (see Figs. 5(a) and 5(b)).

Finally, the superconducting transition temperature (T_s) was measured performing magnetization vs. temperature measurements. The results are summarized in Table I. Two series of samples were grown to test the reproducibility of the results. The same behavior of the T_s as function of the barrier thickness was observed, for both series of samples. The T_s for pure GBCO thin films was discussed in Ref. 26, which was close to 76 K. The results obtained in the bilayers show that the T_s is strongly suppressed when the BTO thickness is increased. There are three possible scenarios to analyze these results. First, the T_s in the bottom electrode could be strongly affected by stress, and the tetragonal distortion, induced by the BTO.[23] The effect could be more relevant for thick BTO insulating layers. Second, as observed from CAFM measurements, the density of pinholes is strongly reduced when the BTO thickness is increased. In this context, deficient oxygen GBCO layers could be obtained as consequence of reduced oxygen diffusion across the BTO. Finally, the strong suppression in T_s could be associated to an interaction between FE and superconductivity, due to spontaneous polarization induced by stress in the BTO layer or proximity effects.[11] Proximity effects in superconducting/ferromagnetic structures have been long discussed in the literature.[40] More studies are necessary to clarify the role of each different mechanism in the T_s reduction. However, GBCO/BTO/GBCO trilayers present different T_s at the bottom (low T_s) and top (high T_s) superconducting electrodes. This fact excludes the scenario of further FE/superconductivity interplay by spontaneous polarization,[11] which indicate that stress (due to substrate and barrier interfaces) and poor oxygenation across the BTO barrier are relevant mechanism for the reduction.[41]

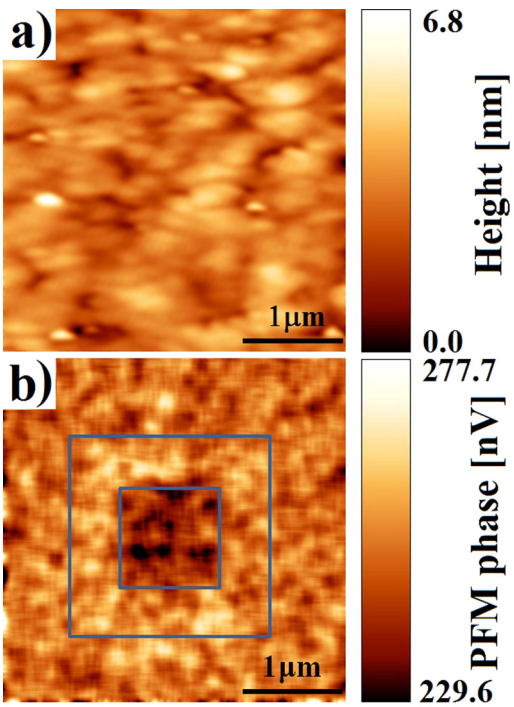

FIG. 5. (a) AFM topographic image in the [G-B-4] bilayer. (b) Bi-domain polarization image obtained in the [G-B-4] bilayer. Contrast indicates the amount of reversed polarization. The center was polarized with +4 V and the middle region with −4 V.

The results obtained show that it is possible to design GBCO/BTO bilayers with potential applications in SIS tunnel junctions. Although the tunnel current is systematically suppressed by increasing the BTO thickness, a careful CAFM study of the barrier homogeneity indicates that BTO thicknesses above 3 nm are necessary for free pinhole barriers. This critical thickness is mainly associated with the surface roughness at the bottom GBCO electrode. Although RMS values around 1 nm can be obtained in very thin GBCO films,[26] the steps at the terrace borders present high conductivity and reduce the performance (by inhomogeneous conductivity) in very thin dielectric layers. On the other hand, a reduction in the T_s of the samples was observed when the BTO thickness is increased. The reduction of the T_s in the GBCO layer is more critical at the GBCO/BTO interface. A reduction of T_s or suppression of the superconductivity at the interfaces (top and bottom for trilayers) can increase the effective thickness for tunneling in the superconducting state. An increment in the barrier thickness should affect the coupling between the superconducting electrodes. On the other hand, the high sensibility of the barrier properties to the oxygen content suggests that the functionality of the barrier can be also tuned by post annealing process. The oxygen vacancies modify the properties at the insulator barrier and should also affect the superconducting properties at the GBCO electrodes.

IV. CONCLUSIONS

Summarizing, a detailed study of the structural, morphological, and electronic properties in GBCO/BTO bilayers has been performed. It was found that the tunnel current is systematically reduced (for equal applied voltage) by increasing the $BaTiO_3$ barrier. The $BaTiO_3$ layers present an energy barrier of $\approx$1.2 eV ($m^* \rightarrow m_e$) and an attenuation length of 0.35–0.5 nm in the range between 3 and 4 V. The GBCO electrode is totally covered by a BTO thickness above 3 nm. The presence of FE was verified by piezoresponse force microscopy (PFM) for a BTO thickness of 4 nm. The T_s of the bilayers is systematically suppressed when increasing the BTO thickness. This can be associated with both stress reducing the orthorhombicity and reduced oxygen stoichiometry (poor diffusion of the oxygen across the $BaTiO_3$ top layer). Both effects could act synergistically reducing the orthorhombicity of the GBCO electrode close to the interface. Bilayers free of direct pinholes with nominal thickness of 16 nm GBCO and 4 nm

BTO with $T_s \approx 48$ K and FE can be obtained. It should be noticed that CAFM can only detect "direct" pinholes, straight holes in the barrier where the conductive tip can contact the bottom electrode. However, it cannot detect "tilted" or "wormlike" pinholes in which the tip cannot contact the bottom electrode. These pinholes could be filled during the deposition of the counter electrode, short-cutting the device for thicknesses lower than expected. The results in the current work contribute to the design of SIS heterostructures based on HTS and FE materials with functionalities out of the temperature range limited by LTS.

ACKNOWLEDGMENTS

This work was partially supported by the ANPCYT (PICT PRH 2008-109), Universidad Nacional de Cuyo (06/C395) and by the Institute for Basic Science (IBS) through the Center for Artificial Low Dimensional Electronic Systems by Project Code (IBS-R015-D1). N.H. is a member of the Instituto de Nanociencia y Nanotecnología (Argentina). M.S. and N.H. are members of CONICET (Argentina).

[1]J. Clarke, W. M. Goubau, and M. B. Ketchen, J. Low Temp. Phys. **25**, 99 (1976).
[2]S. P. Benz and C. A. Hamilton, Appl. Phys. Lett. **68**, 3171 (1996).
[3]K. K. Likharev and V. K. Semenov, IEEE Trans. Appl. Supercond. **1**, 3 (1991).
[4]M. H. Dvoret and R. J. Schoelkopf, Science **339**, 1169 (2013).
[5]J. Zmuidzinas and P. L. Richards, Proc. IEEE **92**, 1597 (2004).
[6]M. Sirena, J. Appl. Phys. **110**, 063923 (2011).
[7]N. Haberkorn *et al.*, Appl. Phys. Lett. **84**, 3927 (2004).
[8]J. Biscaras, N. Bergeal, A. Kushwaha, T. Wolf, A. Rastogi, R. C. Budhani, and J. Lesueur, Nat. Commun. **1**, 89 (2010).
[9]Y. Gim, A. W. Kleinsasser, and J. B. Barner, J. Appl. Phys. **90**, 4063 (2001).
[10]M. van Zalk, M. Veldhorst, A. Brinkman, J. Aarts, and H. Hilgenkamp, Phys. Rev B **79**, 134509 (2009).
[11]A. Crassous *et al.*, Phys. Rev. Lett. **107**, 247002 (2011).
[12]V. Garcia and M. Bibes, Nat. Commun. **5**, 4289 (2014).
[13]V. Lemanov, E. P. Smirnova, P. P. Syrnikov, and E. A. Tarakanov, Phys. Rev. B **54**, 3151 (1996).
[14]V. V. Lemanov, Phys. Solid State **39**, 318 (1997).
[15]S. Saha, T. P. Sinha, and A. Mookerjee, Phys. Rev B **62**, 8828 (2000).
[16]J. F. Schooly, W. R. Hosler, and M. L. Cohen, Phys. Rev. Lett. **12**, 474 (1964).
[17]S. H. Wemple, Phys. Rev. B **2**, 2679 (1970).
[18]K. A. Muller and H. Burkard, Phys. Rev. B **19**, 3593 (1979).
[19]J. H. Haeni *et al.*, Nature **430**, 758 (2004).
[20]K. J. Choi, M. Biegalski, Y. L. Li, A. Sharan, J. Schubert, R. Uecker, P. Reiche, Y. B. Chen, X. Q. Pan, V. Gopalan, L.-Q. Chen, D. G. Schlom, and C. B. Eom, Science **306**, 1005 (2004).
[21]N. Sai, A. M. Kolpak, and A. M. Rappe, Phys. Rev B **72**, 020101 (2005).
[22]G. Gerra, A. K. Tagantsev, N. Setter, and K. Parlinski, Phys. Rev. Lett. **96**, 107603 (2006).
[23]V. Vonka, S. J. van Reeuwijk, J. M. Dekkers, S. Harkema, A. J. H. M. Rijnders, and H. Graafsma, Thin Solid Films **449**, 133 (2004).
[24]B. Wuyts, V. V. Moshchalkov, and Y. Bruynseraede, Phys. Rev. B **53**, 9418 (1996).
[25]N. Haberkorn, G. Bridoux, E. Osquiguil, G. Nieva, and J. Guimpel, Appl. Surf. Sci. **254**, 222 (2007).
[26]H. Navaro, M. Sirena, J. Kim, and N. Haberkorn, Phys. C **510**, 21 (2015).
[27]O. Nakamura, E. E. Fullerton, J. Guimpel, and I. K. Schuller, Appl. Phys. Lett. **60**, 120 (1992).
[28]K. M. Lang, D. A. Hite, R. W. Simmonds, R. McDermott, P. Pappas, and J. M. Martinis, Rev. Sci. Instrum. **75**, 2726 (2004).
[29]M. Sirena, L. Avilés Félix, and N. Haberkorn, Appl. Phys. Lett. **103**, 52902 (2013).
[30]F. Bardou, Europhys. Lett. **39**, 239 (1997).
[31]D. A. Rabson, B. J. Jönsson-Åkerman, A. H. Romero, R. Escudero, C. Leighton, S. Kim, and I. K. Schuller, J. Appl. Phys. **89**, 2786 (2001).
[32]I. C. Infante, F. Sánchez, V. Laukhin, A. Pérez del Pino, J. Fontcuberta, K. Bouzehouane, S. Fusil, and A. Barthélémy, Appl. Phys. Lett. **89**, 172506 (2006).
[33]N. Haberkorn, F. Lovey, A. Condo, and J. Guimpel, J. Appl. Phys. **97**, 53511 (2005).
[34]J. G. Simmons, J. Appl. Phys. **34**, 1793 (1963).
[35]C. N. Berglund and W. S. Baer, Phys. Rev. **157**, 358 (1967).
[36]T. Hirano, M. Ueda, K.-i. Matsui, T. Fujii, K. Sakuta, and T. Kobayashi, Jpn. J. Appl. Phys., Part 2 **31**, L1345 (1992).
[37]D. P. Cann and C. A. Randall, J. Appl. Phys. **80**, 1628 (1996).
[38]I. Pallecchi, G. Grassano, D. Marre, L. Pellegrino, M. Putti, and A. S. Siri, Appl. Phys. Lett. **78**, 2244 (2001).
[39]A. P. Chen, F. Khatkhatay, W. Zhang, C. Jacob, L. Jiao, and H. Wang, J. Appl. Phys. **114**, 124101 (2013).
[40]A. I. Buzdin, Rev. Mod. Phys. **77**, 935 (2005).
[41]N. Navarro *et al.* (unpublished).